Wideband Array-Fed Fabry-Perot Cavity Antenna for 2-D Beam Steering

Wideband Array-Fed Fabry-Perot Cavity Antenna for 2-D Beam Steering

Davide Comite, *Senior Member, IEEE,* Symon K. Podilchak, *Member, IEEE*
Maksim Kuznetcov, *Student Member, IEEE,* Victoria Gómez-Guillamón Buendía, *Member, IEEE,*
Paolo Burghignoli, *Senior Member, IEEE* Paolo Baccarelli, *Member, IEEE*, and Alessandro Galli, *Member, IEEE*

***Abstract*—We propose the design and test of a 2-D Fabry-Perot structure based on a multilayer slab arrangement fed by a circular array of simple sources. Such a class of planar leaky-wave antenna can be made by low-loss commercial laminates and it is bounded on top by a sub-wavelength partially-reflecting surface. The antenna is designed to suppress undesired radiation from the quasi-TEM mode while leaking power by the excitation of a fast TM_1 leaky mode, which is a perturbed version of the guided-wave supported by the corresponding parallel-plate waveguide. An accurate dispersive analysis for the multilayer structure is developed and an original feeding system is designed and optimized to provide the needed wideband impedance matching. Thanks to translational invariance enabled by the homogenized nature of the partially reflecting screen, the antenna is used as a radiating element in the design of a leaky-wave-enhanced phased array, constituted by an arrangement of vertical probes to generate directive pencil beams steerable at a single frequency in azimuth and by changing frequency in elevation.**

***Index Terms*—Phased arrays, Fabry-Perot cavity antennas, beam steering, leaky-wave antennas, cylindrical leaky waves, conical patterns.**

I. Introduction

The future generation of communication, radar, and wireless power-transfer systems demands for the design of high-gain and compact antennas enabling advanced radiation features, such as electronic steering of highly directional beams, pattern and polarization reconfigurability [1], and vortex beams carrying orbital angular momentum [2]. As is well known, conventional techniques for realizing steerable pencil or broadside high-gain beams, possibly characterized by a reconfigurable polarization state, are based on the use of multiple planar radiating elements, each one characterized by low or moderate directivity. They are made by microstrip patch antennas aligned along one or two directions to form an array [3]. Such devices imply high cost and bulky structures and, even if the design of corporate and series-fed networks are well established, they typically require the use of large, often lossy and expensive implementations (see, e.g., [3]). Alternatives techniques have also been proposed in the last decade, such as tunable inductive partially reflective surfaces (PRSs) [4], phase modulated metasurfaces [5], phase transformers [6], [7], slotted structures [8], lenses [9], [10], composite feeding networks [11], and active frequency selective surfaces [12].

An alternative solution to achieve high-gain pencil beams scanning over the 3-D space, providing potentially unlimited reconfigurable features (in terms of polarization and steering) can involve an array of elementary sources such as in 1-D or 2-D leaky-wave antennas (LWAs) [13]–[20], whose dispersion features, following leaky-wave (LW) theory [21], can be flexibly controlled. More importantly, the enhanced directivity provided by LW aperture fields can allow for improved radiating performances, significantly reducing the number of elements and phase shifters required to achieve equivalent beam steering features [16], [17] if compared to more conventional phased array approaches [22].

Fabry-Perot cavity antennas (FPCAs) exploit PRSs for the top aperture (made by a homogenizable, quasi-uniform metal screen) and can be defined as a class of 2-D planar LWA. Contrasted with alternative bull-eye designs (see, e.g., [18], [23] and refs. therein), which are made by non-homogenizable gratings, FPCAs offer translation invariance, which is convenient to embed an array of sources below the PRS for beam steering [17], [19]. In general, by properly designing the cavity, top PRS, and feeder, it is also possible to control the pattern direction and shape, which can be either a broadside pencil beam [24] or a conical beam [25]-[27]. Furthermore, as for all LWAs, the direction of the beam can be controlled by changing the frequency, whereas the feeder is typically a simple, non-directive radiator, such as a printed patch, ground plane slots arrangement, or dipole, working as the launcher of a cylindrical leaky-wave (CLW) [28]. Extensive efforts have also recently been made to achieve high-gain and wideband broadside radiation with such structures [29]–[34].

By taking advantage of the recent improvements in LWA array design, whilst considering more conventional CLW excitation approaches and FPCA design concepts [17]–[28], we discuss and experimentally verify the design of a new multilayer FPCA excited through a wideband feeder that can provide single-frequency beam steering in the far field. The newly reported findings of this paper, in particular, take advantage of the theory developed in [17], where some of the authors numerically demonstrated the possibility of generating a high-gain pencil beam by means of a CLW supported by an

Manuscript received February 25th, 2020, revised May 29th, 2020.
Corresponding author: Davide Comite
This work was partially supported by the European Union's Horizon 2020 Research and Innovation Program through Marie Sklodowska-Curie under Grant 709372.
D. Comite, P. Burghignoli, and A. Galli are with the Department of Information Engineering, Electronics and Telecommunications, "Sapienza" University of Rome, 00184, Rome, Italy (e-mail: davide.comite@uniroma1.it).
S. K. Podilchak is with the Institute of Digital Communications, The University of Edinburgh, Edinburgh EH14 4AS, United Kindom.
V. Gómez-Guillamón Buendía and Maksim Kuznetcov are with the Institute of Sensors, Signals, and Systems, School of Engineering and Physical Sciences Edinburgh Campus, Heriot-Watt University, Edinburgh, UK.
P. Baccarelli is with the Department of Engineering, Roma Tre University, 00182, Rome, Italy.

FPCA. For this theoretical study in [17], the ideal sources were arranged in a square array configuration and properly phased to study the possible steering features. In addition, the FPCA was designed considering a single-layer structure defined by a relative dielectric constant with $\varepsilon_{\rm r} = 1.2$ which might not be easily realizable.

As newly reported in this paper, our proposed and experimentally validated FPCA is constituted by a multilayer (ML) arrangement of commercial laminates (see Fig. 1), which are properly selected to eliminate any spurious radiation produced by the undesired quasi-TEM mode. The feeder is made by a simple vertical probe arrangement, loaded and optimized to provide wideband impedance matching. A circular arrangement of sources is also designed and experimentally validated to form a LW enhanced phased array for beam steering. No similar FPCA has been reported where its dispersive and radiation features have been examined, with such a novel feeding system as well as its single-frequency beam steering capabilities.

Thanks to the leaky-wave mode supported by the structure, the proposed antenna also provides steering in elevation of a directional pencil beam, in contrast with the steering strategies described in [11], [12], where, to achieve azimuth beam steering, a reconfigurable cascaded feeding network connected to endfire radiating elements and an active frequency selective surface were employed.

The aim of this paper is four-fold: i) providing an experimental validation that suppression of spurious radiation related to the unavoidable excitation of the quasi-TEM mode is possible in such structures and assessing the design feasibility through the implementation of a ML slab of commercial laminates; ii) proposing the design of a wide-band omnidirectional feeder for this class of structure, which can be extended to circular or square multi-feed systems for beam steering and polarization control; iii) investigating the attractive features of circular arrays of azimuthal symmetric sources [35], [36], contrasted with a corresponding square arrangement; iv) proposing and experimentally validating the design of an FPCA fed by a thinned circular array of vertical probes [11], [12].

II. Design of the Single Antenna Element

The structure is formed by a ML grounded dielectric slab of total thickness h and relative permittivity $\varepsilon_{{\rm r}_i}$, with $i = 1, .., n$, being n the number of layers, covered on top by a sub-wavelength PRS (see Fig. 1). The major antenna dimension can be described by a total radial aperture $r_{\rm a}$ (that includes the array radius), and it can be excited in the center by a simple source, i.e., a vertical coaxial probe. As discussed in the following, the low-cost nature and the reduced size of this feeder allows for the simple integration of an array of sources within the cavity for beam steering.

The radiation mechanism of the FPCA, when driven by azimuth-symmetric sources, is based on the excitation of the $\rm TM_1$ mode supported by the cavity, a perturbed version of the relevant parallel-plate waveguide mode. It propagates radially as an azimuthally symmetric CLW with complex wavenumber $k_{\rm LW} = \beta - j\alpha$ (see [17], [37], [38]), which is retrieved by performing a dispersive analysis of the structure.

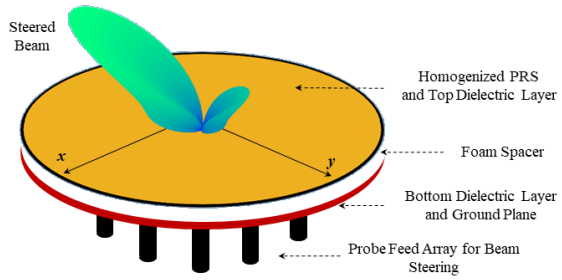

Fig. 1. Representation of the proposed 2-D antenna fed by an array of sources for beam steering. The ML implementation is shown which corresponds to an FPCA with a homogenized PRS defining the top aperture.

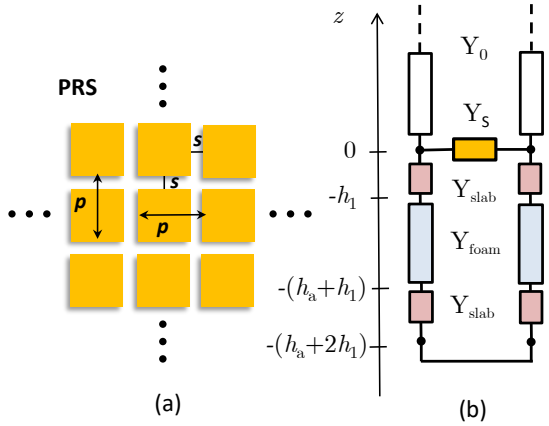

Fig. 2. (a) Detailed geometry of the homogenizable PRS defined by a square lattice of square metal patches with periodicity p and spacing s; (b) TEN of the proposed multilayer FPCA, whose cavity is bounded on top by the PRS. Y_0, $Y_{\rm slab}$, and $Y_{\rm foam}$ are the TM characteristic admittances for the air region, the top and bottom dielectric slabs, and the foam spacer, respectively, while $Y_{\rm S}$ defines the TM admittance for the top PRS as in (a).

A. Modal Analysis of the Multilayer Design

The top of the FPCA is constituted by a periodic arrangement of square metallic patches (shown in Fig. 2(a)) with a square unit cell, sub-wavelength period p, and spacing s, thus forming a PRS having negligible thickness. Such a PRS can be homogenized and thus can be described in terms of a surface (transition) admittance boundary condition $\tilde{\mathbf{J}}_{\rm s}(\mathbf{k}_{\rm t}) = \bar{\mathbf{Y}}_{\rm s}(\mathbf{k}_{\rm t}) \cdot \tilde{\mathbf{E}}_{\tau}(\mathbf{k}_{\rm t})$, where the tilde indicates spectral-domain quantities, $\tilde{\mathbf{J}}_{\rm s}$ is the homogenized surface current on the PRS, and $\tilde{\mathbf{E}}_{\tau}$ is the homogenized electric field tangential to the PRS (and continuous across it). The surface admittance dyadic $\bar{\mathbf{Y}}_{\rm s}$ is obtained considering that the PRS is the Babinet-complementary of a metallic strip grid, which can in turn be described in terms of approximate Kantorovich boundary conditions [39].

The expression of the surface admittance is given by $\bar{\mathbf{Y}}_{\rm s} = Y_{\rm TM}(|k_{\rm t}|)\mathbf{u}_0\mathbf{u}_0 + Y_{\rm TE}(|k_{\rm t}|)\mathbf{v}_0\mathbf{v}_0$, where $\mathbf{u}_0 = \mathbf{k}_{\rm t}/|\mathbf{k}_{\rm t}|$ and $\mathbf{v}_0 = \mathbf{z}_0 \times \mathbf{u}_0$, and it shows that the homogenized PRS is both *translationally* and *rotationally* symmetric, which is an important feature, different, e.g., from more conventional bull-eye LWAs (see, e.g., [23]). In fact, this avoids enforcing any

constraints on the positioning of the feed array, which can be sized to suppress grating lobes and to accommodate a certain number of elementary sources (essentially constrained by their physical encumbrance). In addition, this PRS produces no TM/TE cross-coupling, therefore, when considering a vertical source, the TE part of the dyadic can be neglected and the PRS can be described in terms of a single scalar TM admittance [39], thus greatly simplifying the dispersive analysis of the ML stack.

With an azimuthally symmetric feeder, an azimuthally symmetric CLW can be excited, producing a conical pattern in the far-field [23], [27]. This can be profitably employed as a single-element pattern when considering an array [17]. Also, as discussed in the literature (see, e.g., [40], [41]), undesired radiation from the additional quasi-TEM LW mode, which is a perturbed version of the TEM mode of the parallel-plate waveguide, can be avoided by filling the cavity with a dielectric slab with ε_r suitably larger than 1. This allows for the transformation of the quasi-TEM LW mode into a non-radiating, slow wave [40].

When considering the PRS, the period p should be much smaller than the working wavelength and, for a K-band application, it is chosen here to be 3 mm (with $s = 50$ μm), whereas the substrate and structure dimensions are chosen to radiate at least 90% (96% at 20 GHz) of the power injected into the TM LW mode with the radial aperture r_a of the LWA evaluated as $0.18\lambda k_0/\alpha$ [21]. Moreover, the antenna efficiency is evaluated as $\eta = 1 - e^{-2\alpha(r_a - r_s)}$, r_s being the major radial dimension for a square array for beam steering or the maximum radial size when considering a circular array feeder.

To perform the dispersive analysis, the structure can be represented through a simple transverse equivalent network (TEN see, e.g., [41], and refs. therein), represented in Fig. 2(b). The expression of Y_S can be found in [39], whereas the characteristic admittances of the TM transmission lines (i.e., Y_0, Y_{slab}, and Y_{foam}) are given by conventional transmission line theory when considering TM fields. The modal properties of the Fabry-Perot cavity can then be studied through a dispersion equation, customarily obtained by enforcing the condition of resonance within the TEN in the absence of excitation. The dispersion equation depends on the characteristic admittances, which are functions of the unknown radial wavenumber $k_{LW} = \beta - j\alpha$, to be found numerically with a suitable root-searching algorithm in the complex plane (e.g., the Müller method [42]).

We initially investigated the dispersive features given by a homogeneous slab having $\varepsilon_r = 2.2$. It was observed that adequately low values for the normalized LW attenuation constant (i.e., α/k_0, equal to about 0.05 or less), needed to generate a directive element pattern, were not easily achievable. We thus propose here a new ML configuration made by a stack-up of commercial laminates and foam layers, as shown in Figs. 2(b) and 3, for operation around 21 GHz (which defines a K-band prototype).

The corresponding normalized phase (β/k_0) and attenuation constants for both the TM_1 and the quasi-TEM modes are shown in Fig. 4 both for the ML slab (see figure caption for the relevant details), and for a homogeneous slab with $\varepsilon_r = 1.2$.

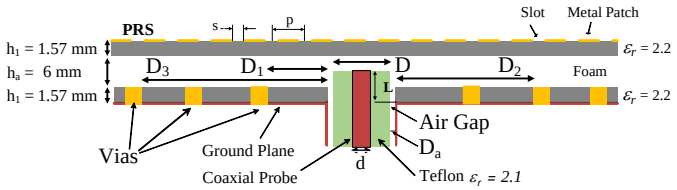

Fig. 3. Feeding system for the single-element ML-FPCA. A double circular arrangement of vertical metallic vias is positioned radially around the active coaxial probe (see Fig. 5). Parameters: D = 0.99 mm, d = 0.31 mm, L = 4 mm. The thickness of the PRS and ground plane is t = 0.035 mm, the radius of the antenna aperture is 12.5 cm. $D_1 = 5$ mm, $D_2 = 10.2$ mm, and $D_3 = 15.3$ mm, and D_a models a very small vertical air gap around the coaxial probe that can occur during fabrication and probe connectivity.

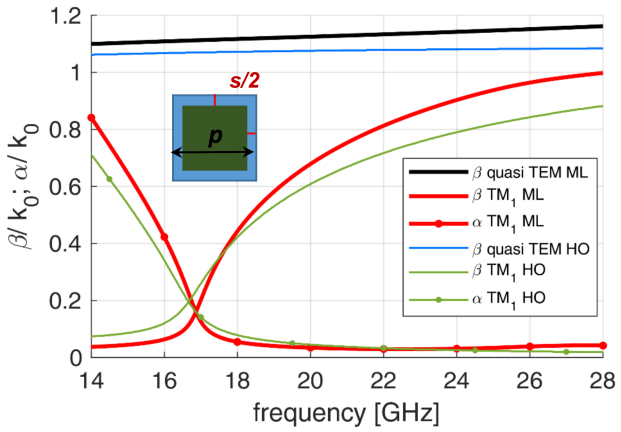

Fig. 4. Dispersion curves for the TEM and TM_1 LW modes supported by the ML FPCA in Fig. 1. The layer thicknesses are given by $h_1 = 1.57$ mm and $h_a = 6$ mm (see Fig. 3). A comparison is also made to a homogeneous (HO) slab with ε_r = 1.2 and total thickness h of 9.14 mm. The inset reports a description of the unit cell of the homogenizable PRS (green metal and blue slot region).

The behavior of β/k_0 for the TM_1 mode of the ML design appears quite similar to that supported by the homogeneous structure, thus confirming the possibility of synthesizing an effective ε_r slightly greater than 1 through low-cost standard laminates. As regards the TEM mode, it is transformed by the dielectric into a bound wave, whose contribution to the far-field radiation will be shown to be negligible, provided that absorbing materials are used at the antenna truncation [38].

The results in Fig. 4 also demonstrate that the dispersive features of the ML structure are not significantly different from those of the homogeneous slab. By analyzing Fig. 4 and considering the symmetric properties of the azimuthally invariant FPCA excited by a vertical probe, one can readily determine the scanning behavior of the omnidirectional conical beam by following [17]. Also, broadside radiation is not generally possible when launching a CLW with a vertical probe, therefore the minimum possible scanning angle close to broadside (i.e., θ_{min}) is limited by the low-frequency cut off of the LW, occurring at $\beta = \alpha$. By increasing the frequency, the beam scans towards endfire and, when $\beta > \alpha$, the beam angle can be estimated through the standard relation $\theta_p \simeq \sin^{-1}(\beta/k_0)$ [21]. The maximum allowed scanning angle

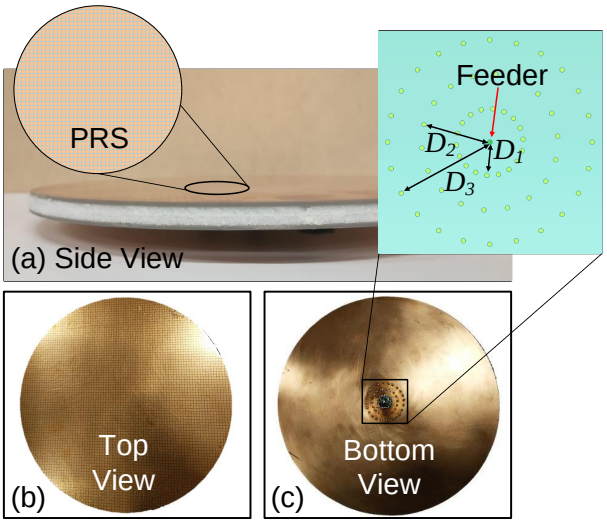

Fig. 5. Manufactured prototype: (a) side view showing the ML stack, (b) top view showing the sub-wavelength PRS made by the square patches, and (c) bottom view showing the coaxial probe (part no. PE44217, from Pasternack Inc.) and arrangement of vias for the single-element LWA.

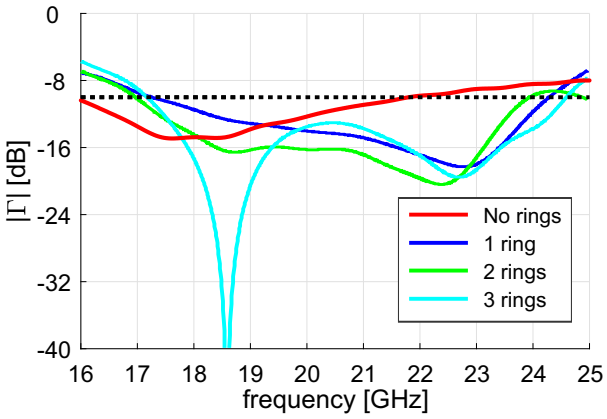

Fig. 6. Simulated reflection coefficients for the single-element FPCA considering an ideal probe and the various via rings defined by the appropriate radius; i.e., D_1, D_2, and D_3. It can be observed that the reflection coefficient is not well matched over the entire band from 17 to 23 GHz when no rings are included. However, matching improves over this frequency range as the number of via rings increases, for example, achieved reflection coefficient values are -10 dB (or better) with 2 and 3 via rings.

close to endfire is mainly related to the cutoff of the first higher-order TM leaky mode; i.e., the TM_2 mode. These features define a wideband operational frequency range for the FPCA.

B. Single Probe Feeding System

The ML FPCA is fed with a vertical coaxial probe penetrating the cavity through the ground plane. By adjusting the probe length and, thus, its penetration, we have initially observed it was not possible to achieve satisfactory wideband impedance matching (with $|\Gamma|$ not well below -8 or -10 dB, see Fig. 6) around the central frequency chosen here to be 21 GHz, according to Fig. 4. To overcome this limitation, we have investigated different loading layouts and propose herein an original circular arrangement of short vertical vias accommodated within the bottom laminate. As a result of this reactive loading the impedance matching is more centered around 21 GHz, as desired, when the via rings are added. More specifically, it can be observed that the impedance bandwidth does have a frequency shift (where $|\Gamma| < -10$ dB) starting from 16 GHz to about 17 GHz for the cases with and without via rings, respectively. This ensures a better matching centered around the design frequency of 21 GHz.

As shown in Fig. 3, the via layout for the single-element FPCA is composed of three concentric circles and it has been properly sized to ensure manufacturing simplicity. The values of the radii of the three circles ($D_1 = 5$ mm, $D_2 = 10.2$ mm, and $D_3 = 15.3$ mm) visible in Fig. 3 have been optimized considering an initial value equal to $\lambda_g/4$, λ_g being the wavelength for the guided mode at 18 GHz. Also, for low-cost manufacturing and design simplicity the vias were chosen to have a diameter of 1 mm while the via height was enforced by the thickness of the bottom substrate. The total via number along the two more internal circles was selected to be 18 while the ones for the external circle were set to 24. Some vias can be eliminated and replaced with other feed points for beam steering by considering LWA phased array approaches [16], [17], as demonstrated in the next sections for the proposed and experimentally verified ML FPCA.

When the centrally positioned probe is not surrounded by the three via rings, the reflection coefficient values are greater than -10 dB at about 21 GHz and above (see Fig. 6). With the introduction of the first via ring (having radius D_1) the reflections are reduced (i.e., $|\Gamma|$ is about -20 dB) and a particular resonance concentrated near the vias can be observed in the simulations (see Fig. 7). With the introduction of the other rings positioned at D_2 and D_3 the antenna reflections can be further reduced over entire range from about 18 to 23 GHz.

To investigate this phenomenon further, the simulated electric field on the ground plane containing the top surface of vias are reported in Fig. 7. It can be observed that a strong resonance over the first ring, which is related to the high concentration of current near the rings, can indeed improve the matching. For example, such resonances can be well observed at about 18.3 GHz where all rings at D_1, D_2 and D_3 show a strong concentration of field. This is related to the reflection coefficient minimum at this same frequency as shown in Fig. 6. Analyzing the surface current on the ground plane (not reported here), at some mid-band frequencies, i.e., at 19.5 and 20.5 GHz, a current concentration on the two outer via rings was not observed, yet matching is still less than -10 dB due to the standing wave created between the central probe and the first via ring, thus improving matching beyond the case when no vias were present.

III. Characterization of the Single-Element LWA

We describe here the performance and radiation features of the manufactured ML design (shown in Fig. 5) by exciting the antenna with the optimized feeder presented in Fig. 3.

The impedance matching for a coaxial probe positioned at the origin is shown in Fig. 8, where an excellent agreement

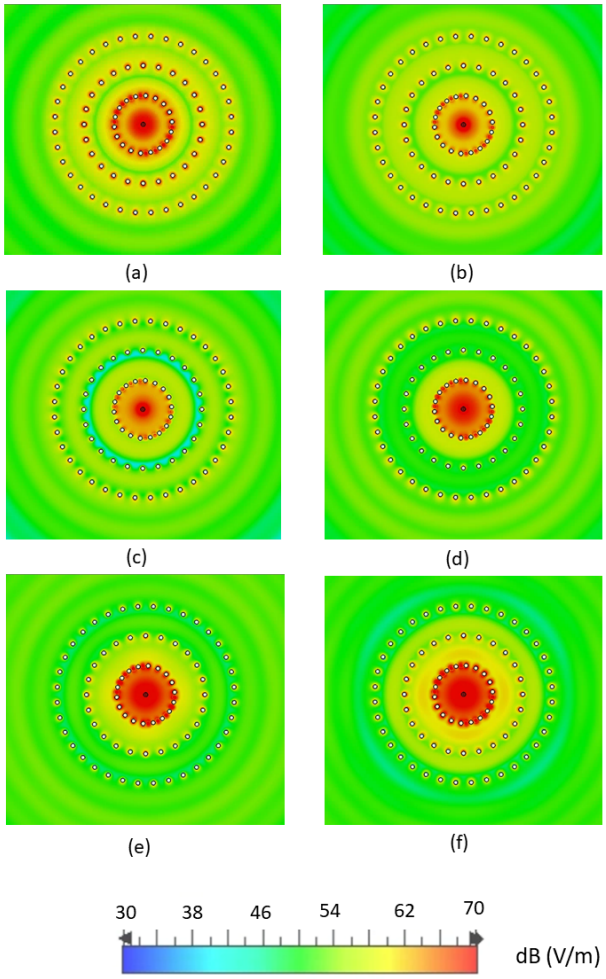

Fig. 7. Simulated electric field (absolute value) on the xy plane placed just on top of the via rings from 18 GHz to 23 GHz, at step of 1 GHz (panels (a) to (f)). Resonances can be observed providing the good matching performances. A strong surface current distribution can be observed (not reported here) generating the improved impedance matching as compared to the case when no via rings were present (see Fig. 6).

between full-wave and experimental results is observed. As desired, wideband impedance matching, from about 17 GHz to 23.5 GHz, has been achieved for the FPCA. These good matching values can be explained by the resonance introduced by the via arrangement. For example, $|\Gamma| < -30$ dB at about 18.5 GHz and 22.3 GHz for the simulations. For comparison, feed system matching without the vias is also shown.

Figure 8 also provides a comparison between the measured and simulated maximum value of the realized gain for the conical beam. A good agreement is observed over the entire frequency range, with a minor variation related to measurement practicalities (i.e., phase offsets due to cable bending, possible scattering from the antenna tower and other non-ideal effects), which was smaller than about 2 dB. The antenna radiates a vertically polarized beam; cross-polarization levels, mainly determined by depolarization effects at the truncation (not reported here due to space limitations), are at least -20 dB below the co-pol field.

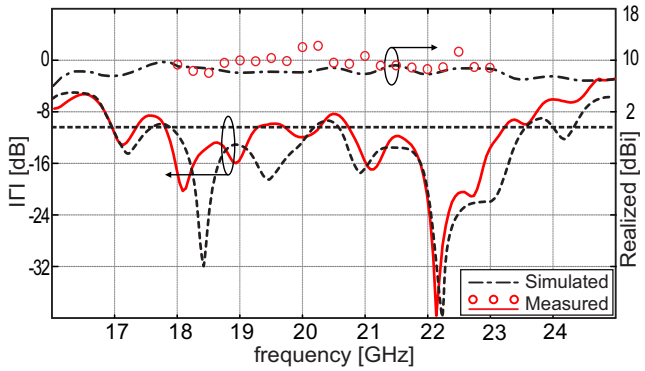

Fig. 8. Reflection coefficient (left axis) of the FPCA fed through the system described in Figs. 3 and 5. The horizontal dotted black line indicates the conventional -10 dB matching threshold. The simulation model also included the connector and all fabricated tolerances for the practically realized LWA (such as the air gap around the probe, etc. see Fig. 3) providing a good comparison with the fabricated and measured prototype. Realized gain over frequency (right axis) for the ML antenna where values of about 10 dB_i can be observed defining an α with relatively low dispersion.

The normalized 2-D polar representation of the radiation pattern for the single-fed FPCA antenna, for a discrete number of frequencies corresponding to the realized gain in Fig. 8, is plotted in Fig. 9. Eight different frequencies have been reported (see figure caption for all the relevant details), which show an omnidirectional conical beam scanning with frequency over the zenith angle (i.e., θ), following the dispersive features of the LW mode (see Fig. 4). A comparison over a single azimuth cut is also reported in Fig. 10, showing good agreement between simulations and measurements. Also, by following LW theory and our developed dispersive analysis (see Fig. 4), the numerically calculated beam angle, θ_p, can be compared to the measurements as in Fig. 11 up to 25 GHz. It can be observed that results are in good agreement. On this basis, we can safely conclude that the presence of vias can indeed improve the impedance matching without significantly perturbing the propagation of the leaky mode.

It should be mentioned that we report radiation patterns up to 23 GHz in Fig. 10 since the patterns quickly degraded after this value. In particular, a clear and distinct conical beam pattern cannot easily be identified. However, this is not due to a dramatic degradation of the gain, which keeps essentially stable thanks to the LW field that dominates the antenna aperture, nor the poor impedance matching (see Fig. 8 which shows results up to 25 GHz). The degradation, instead, is related to the presence of spurious contributions which radiate at the antenna truncation, and that become stronger at higher frequencies. To rectify this problem, a larger antenna aperture is required to reduce the effects of the spurious radiation near endfire. However, we were not able to easily fabricate and measure a larger structure in our laboratory. For this reason, we have optimized the antenna size and upper frequency, to be about 23 GHz.

IV. Array Design and Performance

Thanks to the translational invariance of the developed structure it is possible to embed more sources within the cavity

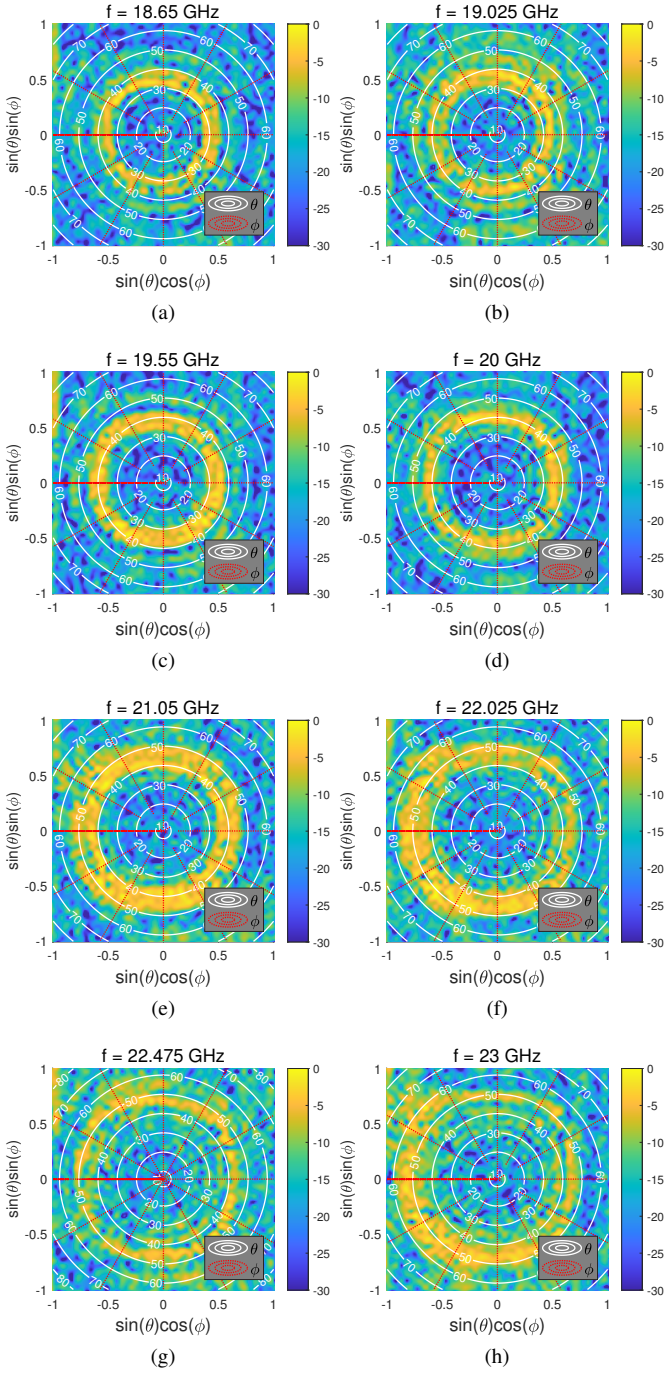

Fig. 9. Normalized contour maps (dB) of the measured electric field (E_θ) defining a conical beam pattern for the antenna structure in Fig. 5. Different frequencies (from (a) to (h)) are reported from 18.65 GHz to 23 GHz. The angle ϕ is measured with respect to the horizontal axis.

to form a circular [35] or square lattice of feed points. In particular, this class of FPCA can adopt array thinning concepts [16] while also neutralizing the conventional gain losses of the beam when scanning towards end-fire [17]. In this section we present the design of an array feeder for the excitation of the proposed FPCA, based on commercial coaxial probes. The radiation features provided by the circular arrangement of azimuth-symmetric sources, obtained by processing the measured data, will also be discussed in the following.

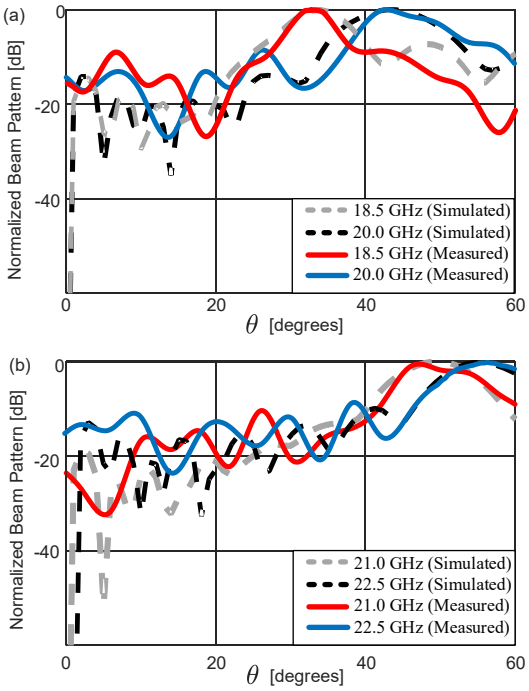

Fig. 10. Beam patterns ($\phi = 0°$ plane) for the measured FPCA (see Fig. 5).

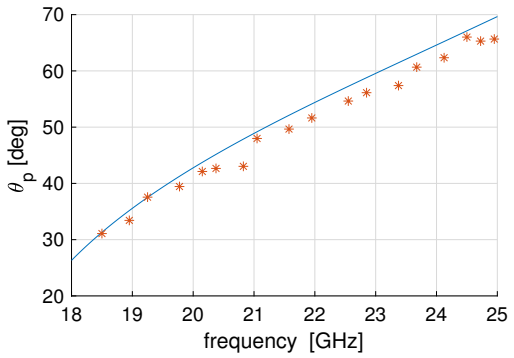

Fig. 11. Beam pointing direction θ_p for the FPCA prototype (see Fig. 5). Solid line: model; Asterisks: measurements.

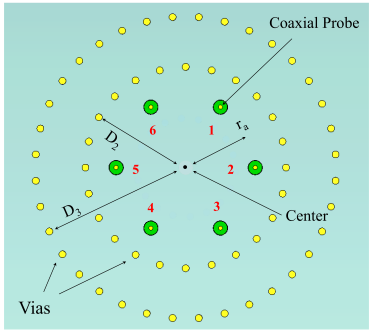

Fig. 12. Probe and via positioning for the proposed circular-array feeder which excites the FPCA presented in Fig. 5 for beam steering. The 6-port feed system, which is constituted by commercial probes, is surrounded by two circles of vertical vias (defined by D_2 and D_3) which provide wideband impedance matching and low coupling values between the ports.

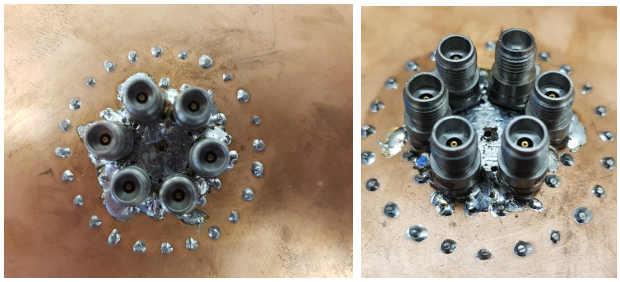

Fig. 13. Bottom view and perspective view of the fabricated and measured array feeder system for the FPCA defined in Fig. 5(a) and (b).

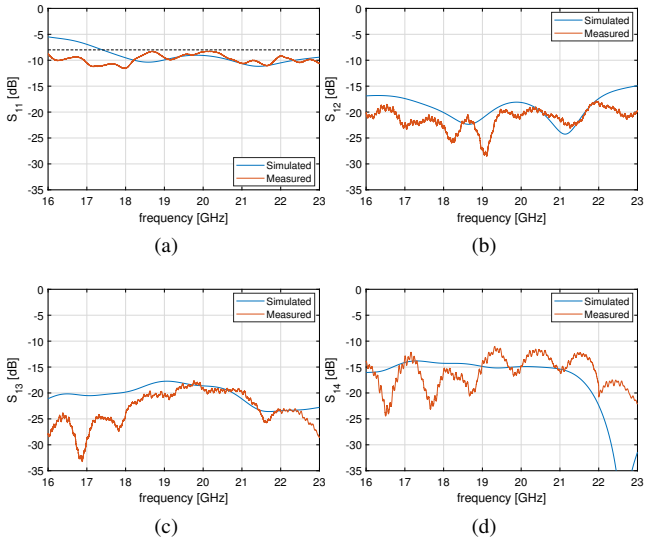

Fig. 14. Amplitude of the simulated and measured scattering parameters (in dB) of the array fed by a circular array of 6 probes (see Fig. 13). Thanks to the circular symmetry of the structure only a subset of all parameters has been reported. The horizontal black dashed line in panel (a) indicates the -8 dB value.

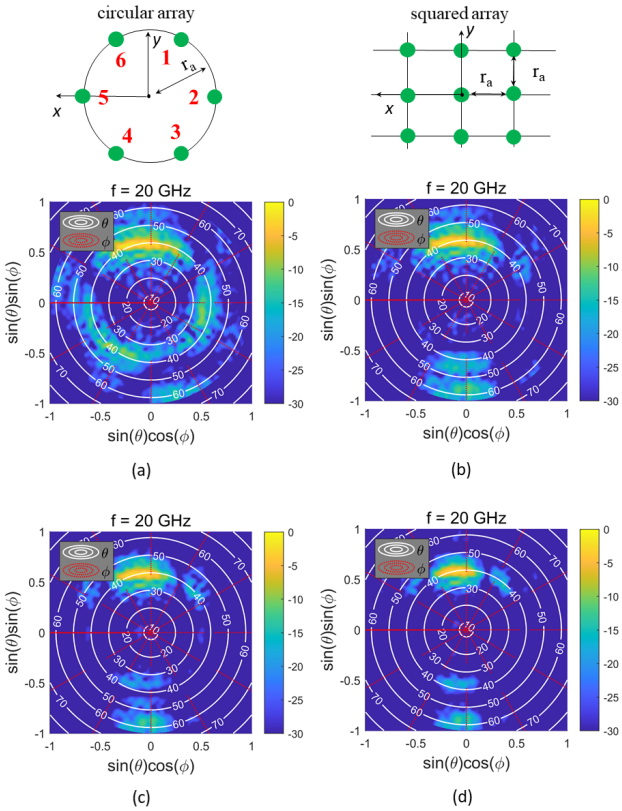

Fig. 15. Normalized contour maps (dB) for E_θ of the array pattern using measured data at 20 GHz where the feed array is phased to scan at the azimuth angle $\phi_0 = 100^\circ$ (other main beam angles are possible by following [17]): (a) circular feeding array of 6 sources, (b) square lattice array using a 3×3 feed system, (c) similar to (b) but with a 4×4 feed source arrangement, and (d) 5×5 square array of sources. The top panel reports the corresponding geometrical configuration of the array sources (depicted in green color).

The design of the circular array feeder (see Fig. 12) is constrained by the size of the single elements and by the performance requirements on the side lobes. As is well known from conventional array theory [3], the synthesized beam pattern will have enhanced directivity (thus lower levels of the first side lobe) by increasing the number of antenna elements or sources (see also [17]). At the same time, the total via number within a circle for the feeder (see for example Fig. 12, and probes labeled 1 to 6), is constrained by its radial dimension, which should also be sized to avoid grating lobes (i.e., a radial distance $r_a = 0.5\lambda$ should be maintained, see Figs. 12 and 13). This condition can be anyway slightly relaxed when directive beam patterns are realized by the single antenna element, as outlined in [17]. Basically, there is a compromise in terms of reduced electromagnetic coupling between the elements within the probe arrangement, optimal matching, and feasible mechanical positioning near the origin. Improved matching is possible by placing the probes at a further distance apart, however, grating lobes would be more prevalent at higher frequencies, which we are trying to avoid in this practical implementation for proof-of-concept.

We consider the same commercial coaxial probes as presented in Fig. 5; i.e., part no. PE44217 from Pasternack Inc., which were placed at a radial distance $r_s = 10$ mm. This radial separation represents a major trade-off between the condition on the grating lobes as well as the total encumbrance for the selected commercial probes. Under these conditions, a total number of 6 probes can be accommodated. Moreover, to manufacture the proposed 6-port feed system, the flange screw mount backing for each connector was mechanically reduced in size (original major dimension of 15.9 mm was made to be about 7 mm) to make sure all the connectors could be placed near the origin while also being able to support the required loads and cable connections during measurements. The resulting circular arrangement is defined in Fig. 12, where the relevant port numbering and via placements are detailed for the 6-port feeder while the corresponding manufactured array prototype (bottom side) is shown in Fig. 13.

Figure 14 shows a comparison among simulated and measured scattering parameters of the array. Due to the circular symmetry of the structure only a subset of parameters have been reported. It can be indeed assumed that $S_{ij} = S_{11}$, with $i = j$, and that $S_{16} = S_{12}$ and $S_{15} = S_{13}$. Moreover, similar relations for the other cross coupling parameters can be defined (all reflection and port coupling values not reported

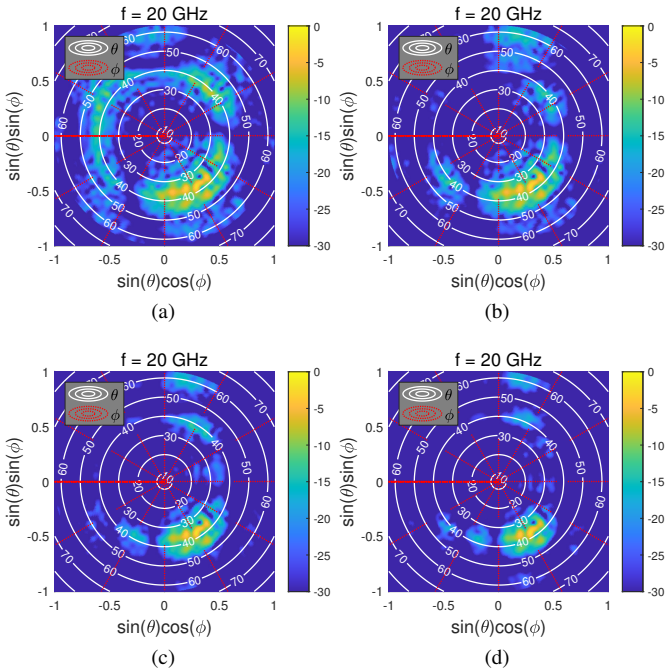

Fig. 16. Normalized contour maps (dB) for E_θ of the array pattern, as in Fig. 15 but phasing to scan at the azimuth angle $\phi_0 = 300°$: (a) circular feeding array of 6 sources, (b) square lattice array using a 3×3 feed system, (c) similar to (b) but with a 4×4 feed source arrangement, and (d) 5×5 square array of sources.

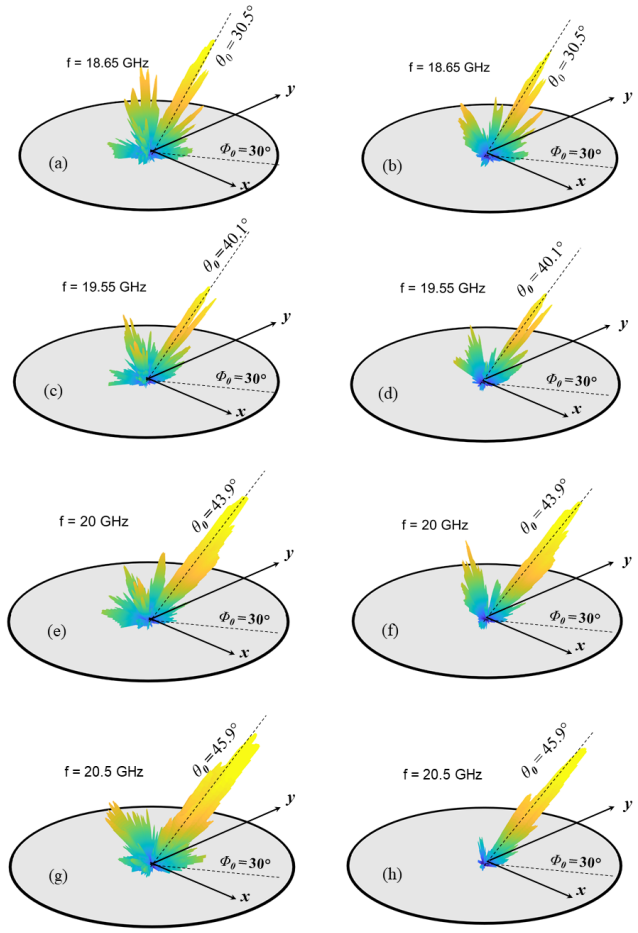

Fig. 17. 3-D patterns (dB, color scale as in Fig. 15 and normalized) of the FPCA array at four different frequencies using measured data of the element in Fig. 5, with $\phi_0 = 30°$: (a), (c), (e), (g) feed configuration for the circular array as in Fig. 15(a); (b), (d), (f), (h) feed configuration for square array as in Fig. 15(b) where reduced SLL can be observed ($r_a = 10$ mm).

due to brevity). In addition, the full-wave simulations show that reduced mutual coupling effects between the ports has been achieved for the optimized and experimentally verified array. This is evident in the results reported in Fig. 14 which are generally below -15 dB for the $|S_{ij}|$ parameters.

Alternative and more complicated feeding approaches are possible to improve the impedance matching and isolation for the elements within the array. For example, this could be based on the use of passive metallic elements, having arbitrary shape, to be placed among the array of sources. This would provide the needed degrees of freedom and could compensate for any undesired capacitive and inductive effects whilst also providing a mechanism to possibly shield the elements for improved isolation. Regardless, the impact of the mutual coupling on the pattern shape and directivity has also been studied for both a circular and square arrangement of sources (see caption of Fig. 15): for instance, minor reductions from the pattern maximum of about 1 dB and of about 2 dB, respectively, have been observed.

We mention that, for simplicity and proof of concept, the FPCA structure in Fig. 5 was re-used to construct the final FPCA array (Fig. 13). To this aim the central feeder and the internal ring of vias were removed to allow for positioning and soldering of the new probes to the ground plane. This final probe arrangement for the array was also important during measurements to ensure clearance for the connectors, cables, and matched loads. This practical implementation was associated to an extensive full-wave simulation and optimization analysis, performed by considering different circular distributions and via sizes for the two remaining via rings. Since a significant performance improvement was not observed during this study, in that $|S_{11}|$ was maintained below -8 dB, the same ring layout (defined by D_2 and D_3) was adopted as in Figs. 3 and 5 for the final array prototype. This probe and via arrangement was also found to be acceptable since the measured $|S_{11}|$ is around -10 dB over the considered frequency range (see Fig. 14(a)).

We next assess the array performance considering the circular array of sources, contrasted with a square arrangement having mutual distances between sources of 8 mm, while employing the array factor as in [17, Eq. (3)]. Figure 15 reports the far-field pattern of various circular and a square arrays at one frequency, phasing the source arrangement to radiate at $\phi_0 = 100°$ (see [17] for the equations needed to get the corresponding complex-valued feeding coefficient), whereas the zenith angle is controlled by frequency following LW theory. Thanks to the directional features of the element pattern (see Fig. 9), a steered and directive pencil beam can be achieved. Normalized contour maps in Figs. 15(b)-(d) show more focused beams, achieved at expense of an increased number of sources and with a non-regular behaviour of the

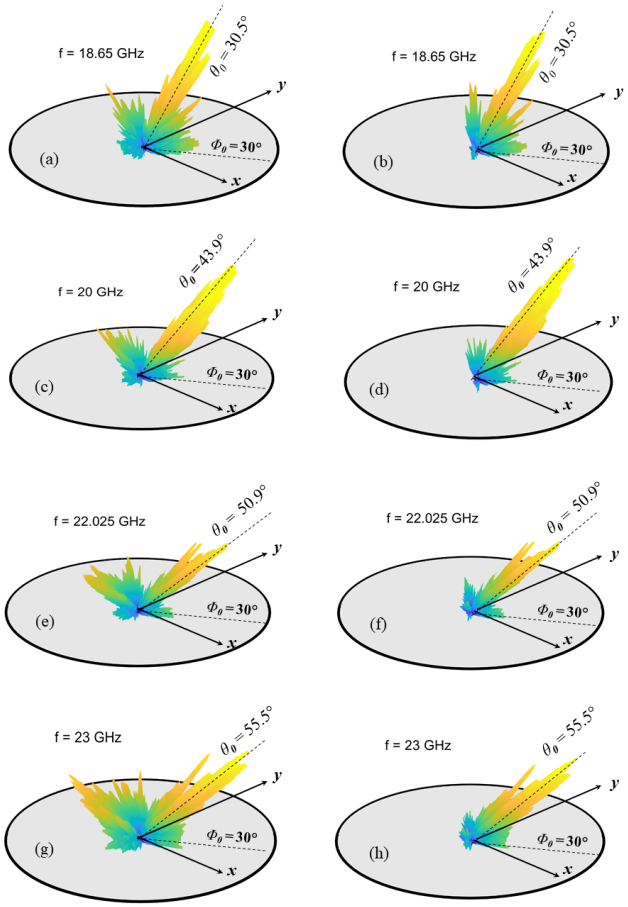

Fig. 18. As in Fig. 17 but for $r_a = 8$ mm.

level of the first sidelobe [17]. Similar patterns have been achieved in Fig. 16 by applying the required phasing to get the beam at $\phi_0 = 300°$, while other results can be estimated at other frequencies where the position of the main beam is defined by ϕ_0 and θ_p.

Figures 17(a)–(h) report a 3-D representation of the measured far field at different frequencies and when the beam is steered to $\phi_0 = 30°$ (see caption for more details). As visible, the side-lobe levels (SLLs) gradually increase while scanning the beam towards end-fire, especially for the circular feeder (values of about -8 dB with respect to the maximum have been achieved). This is, however, an intrinsic challenge with this type of circular array [36] (similar performance with relatively high sidelobes can be also observed in [4] and [5]).

For comparison, we report in Figs. 18(a)–(h) the beam achieved setting $r_a = 8$ mm, which enables the generation of a pencil beam with SLL of about -8 dB up to 23 GHz, where the level of the highest lobe is at about -5 dB for the circular array.

Figure 19 shows the simulated maximum value of the directivity for the circular array. About 14.8 dB_i has been observed for the total pattern and, more importantly, a regular constant level of the first sidelobe versus the azimuth direction of the beam (i.e., ϕ_0) is achieved (about -7 dB and -9 dB, as reported in Fig. 19, for a circular array of 6, 8, and 10 elements). This is contrasted with the stronger variation observed for the square lattice (not reported here, see [17]) due to the lack of circular symmetry. Note that these values for the SLLs are intrinsic to circular arrays (see, e.g., [35]) and can be improved considering advanced techniques [36], which are applicable to this case maintaining the array thinning benefit.

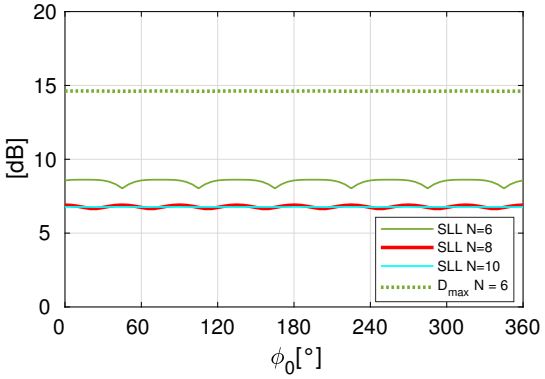

Fig. 19. Simulated maximum directivity (D_{max}), at 20 GHz, and levels of the first side lobe versus the azimuth angle of the steered beam phasing N circular array elements. For $N > 5$, D_{max} keeps the same value.

V. Conclusion

A directive pencil beam steerable in elevation and azimuth has been generated by means of a circular phased array of elementary sources placed inside a wideband FPCA. The dispersion features and measurements of the basic antenna structure have also been reported. In particular, the design of a novel, wideband, integrated feeder for the single antenna element has been outlined. Following these developments, the design of a compact feed system realizing a circular array with 6 ports for LW beam steering, has also been optimized and experimentally validated. The key element of the proposed approach is the exploitation of the directional LW element pattern; i.e., an omnidirectional conical beam characterized by a zeroth-order CLW.

This aperture distribution is supported by the developed multilayer structure, which has also been optimized to suppress radiation of the undesired quasi-TEM mode within the cavity. Overall, the array is planar and wideband, offering the possibility of steering a pencil beam off broadside, and along the azimuth at a fixed frequency, with a reduced number of sources when compared to more conventional 2-D planar arrays.

References

[1] R. L. Haupt and M. Lanagan, "Reconfigurable antennas," *IEEE Antennas Propag. Mag.*, vol. 55, no. 1, pp. 49–61, Feb. 2013.

[2] M. Veysi, C. Guclu, F. Capolino, and Y. Rahmat-Samii, "Revisiting orbital angular momentum beams: Fundamentals, reflectarray generation, and novel antenna applications," *IEEE Antennas Propag. Mag.*, vol. 60, no. 2, pp. 68–81, 2018.

[3] R. C. Hansen, *Phased Array Antennas*. Hoboken, NJ: John Wiley & Sons, 2nd ed., 2009.

[4] A. Ghasemi, and S. N. Burokur, and A. Dhouibi, and A. de Lustrac, "High beam steering in Fabry–Perot leaky-wave antennas," *IEEE Antennas Wireless Propag. Lett.*, vol. 12, pp. 261–264, 2013.

[5] B. Ratni, and W. A. Merzouk, and A. de Lustrac, and S. Villers, and G.-P. Piau, and S. N. Burokur, "Design of phase-modulated metasurfaces for beam steering in Fabry–Perot cavity antennas," *IEEE Antennas Wireless Propag. Lett.*, vol. 16, pp. 1401–1404, 2016.

[6] M. U. Afzal and K. P. Esselle, "Steering the beam of medium–to–high gain antennas using near-field phase transformation," *IEEE Trans. Antennas Propag.*, vol. 65, no. 4, pp. 1680–1690, Apr. 2017.

[7] A. A. Baba, R. M. Hashmi, K. P. Esselle, M. Attygalle, and D. Borg, "A millimeter-wave antenna system for wideband two-dimensional beam steering," *IEEE Trans. Antennas Propag.*, pp. 1–1, 2020.

[8] K. Tekkouk, J. Hirokawa, R. Sauleau, and M. Ando, "Wideband and large coverage continuous beam steering antenna in the 60-GHz band," *IEEE Trans. Antennas Propag.*, vol. 65, no. 9, pp. 4418–4426, Sep. 2017.

[9] X. Zhao, C. Yuan, L. Liu, S. Peng, Q. Zhang, L. Yu, and Y. Sun, "All-metal beam steering lens antenna for high power microwave applications," *IEEE Trans. Antennas Propag.*, vol. 65, no. 12, pp. 7340–7344, Dec. 2017.

[10] E. B. Lima, S. A. Matos, J. R. Costa, C. A. Fernandes, and N. J. G. Fonseca, "Circular polarization wide-angle beam steering at Ka-band by in-plane translation of a plate lens antenna," *IEEE Trans. Antennas Propag.*, vol. 63, no. 12, pp. 5443–5455, Dec. 2015.

[11] P.-Y. Wang, and T. Jin, and F.-Y. Meng, and Y.-L. Lyu, and D. Erni, and Q. Wu, and L. Zhu, "Beam switching antenna based on a reconfigurable cascaded feeding network," *IEEE Trans. Antennas Propag.*, vol. 66, no. 2, pp. 627–635, Feb. 2017.

[12] L. Zhang, and Q. Wu, and T. A. Denidni, "Electronically radiation pattern steerable antennas using active frequency selective surfaces," *IEEE Trans. Antennas Propag.*, vol. 61, no. 12, pp. 6000–6007, Dec. 2013.

[13] P. Baccarelli, P. Burghignoli, F. Frezza, A. Galli, and P. Lampariello, "Novel modal properties and relevant scanning behaviors of phased arrays of microstrip leaky-wave antennas," *IEEE Trans. Antennas Propag.*, vol. 51, no. 12, pp. 3228–3238, Dec. 2003.

[14] H. V. Nguyen, S. Abielmona, A. Rennings, and C. Caloz, "Pencil-beam full-space scanning 2D CRLH leaky-wave antenna array," in *2007 Inten. Symp. Signals Sys. Electronics*, Jul. 2007, pp. 139–142.

[15] M. D. Enders, J. H. Choi, and J. K. Lee, "Integrated full-hemisphere space-to-frequency mapping antenna with CRLH stripline feed network," *IEEE Trans. Microwave Theory Tech.*, no. 99, pp. 1–8, Nov. 2018.

[16] R. Gardelli, M. Albani, and F. Capolino, "Array thinning by using antennas in a Fabry–Perot cavity for gain enhancement," *IEEE Trans. Antennas Propag.*, vol. 54, no. 7, pp. 1979–1990, Jul. 2006.

[17] D. Comite, P. Burghignoli, P. Baccarelli, and A. Galli, "2-D beam scanning with cylindrical-leaky-wave-enhanced phased arrays," *IEEE Trans. Antennas Propag.*, vol. 67, no. 6, pp. 3797–3808, 2019.

[18] D. Comite, S. K. Podilchak, P. Baccarelli, P. Burghignoli, A. Galli, A. P. Freundorfer, and Y. M. M. Antar, "Design of a polarization-diverse planar leaky-wave antenna for broadside radiation," *IEEE Access*, vol. 7, pp. 28 672–28 683, 2019.

[19] D. Comite, V. Gómez-Guillamón Buendía, P. Burghignoli, P. Baccarelli, S. Podilchak, and A. Galli, "Array-fed Fabry-Perot cavity antenna for two-dimensional beam steering," in *2018 IEEE Int. Symp. Antennas Prop. & USNC/URSI National Radio Science Meeting*, 2018, pp. 1873–1874.

[20] F. Costa, D. Bianchi, A. Monorchio, and G. Manara, "Linear Fabry-Perot/leaky-wave antennas excited by multiple sources," *IEEE Trans. Antennas Propag.*, vol. 66, no. 10, pp. 5150–5159, Oct. 2018.

[21] D. R. Jackson and A. A. Oliner, "Leaky-wave antennas," in *Modern Antenna Handbook*, C. A. Balanis, Ed. Hoboken, NJ: John Wiley & Sons, 2008, ch. 7, pp. 325–367.

[22] R. Garg, P. Bhartia, I. J. Bahl, and A. Ittipiboon, *Microstrip Antenna Design Handbook*. Artech house, 2001.

[23] D. Comite, V. Gómez-Guillamón Buendía, S. K. Podilchak, D. Di Ruscio, P. Baccarelli, P. Burghignoli, and A. Galli, "Planar antenna design for omnidirectional conical radiation through cylindrical leaky waves," *IEEE Antennas Wireless Propag. Lett.*, vol. 17, no. 10, pp. 1837–1841, Oct. 2018.

[24] G. Lovat, P. Burghignoli, and D. R. Jackson, "Fundamental properties and optimization of broadside radiation from uniform leaky–wave antennas," *IEEE Trans. Antennas Propag.*, vol. 54, no. 5, pp. 1442–1452, May 2006.

[25] C. A. Allen, C. Caloz, and T. Itoh, "Leaky-waves in a metamaterial-based two-dimensional structure for a conical beam antenna application," in *IEEE MTT-S Int. Microwave Symposium Digest*, vol. 1. IEEE, 2004, pp. 305–308.

[26] D. K. Karmokar, K. P. Esselle, T. S. Bird, and S. G. Hay, "Conical beaming using simple arrays of uniform half-width microstrip leaky-wave antennas," in *4th Asia-Pacific Conf. Antennas Propag. (APCAP)*. IEEE, 2015, pp. 90–91.

[27] C. Caloz, T. Itoh, and A. Rennings, "CRLH metamaterial leaky-wave and resonant antennas," *IEEE Antennas Propag. Mag.*, vol. 50, no. 5, pp. 25–39, Oct. 2008.

[28] A. Ip and D. R. Jackson, "Radiation from cylindrical leaky waves," *IEEE Trans. Antennas Propag.*, vol. 38, no. 4, pp. 482–488, Apr. 1990.

[29] C. Mateo-Segura, A. P. Feresidis, and G. Goussetis, "Bandwidth enhancement of 2-D leaky-wave antennas with double-layer periodic surfaces," *IEEE Trans. Antennas Propag.*, vol. 62, no. 2, pp. 586–593, Feb. 2014.

[30] N. Wang, J. Li, G. Wei, L. Talbi, Q. Zeng, and J. Xu, "Wideband Fabry–Perot resonator antenna with two layers of dielectric superstrates," *IEEE Antennas Wireless Propag. Lett.*, vol. 14, pp. 229–232, 2015.

[31] P.-Y. Qin, L.-Y. Ji, S.-L. Chen, and Y. J. Guo, "Dual-polarized wideband Fabry–Perot antenna with quad-layer partially reflective surface," *IEEE Antennas Wireless Propag. Lett.*, vol. 17, no. 4, pp. 551–554, 2018.

[32] D. Comite, S. K. Podilchak, P. Baccarelli, P. Burghignoli, A. Galli, A. P. Freundorfer, and Y. M. M. Antar, "Analysis and design of a compact leaky-wave antenna for wide-band broadside radiation," *Scientific Rep.*, vol. 8, no. 1, pp. 1–14, 2018.

[33] A. T. Almutawa, A. Hosseini, D. R. Jackson, and F. Capolino, "Leaky-wave analysis of wideband planar Fabry-Perot cavity antennas formed by a thick PRS," *IEEE Trans. Antennas Propag.*, vol. 67, no. 8, pp. 5163–5175, Aug. 2019.

[34] A. Lalbakhsh, M. U. Afzal, K. P. Esselle, and S. L. Smith, "Wideband near-field correction of a Fabry–Perot resonator antenna," *IEEE Trans. Antennas Propag.*, vol. 67, no. 3, pp. 1975–1980, Mar. 2019.

[35] N. Goto and Y. Tsunoda, "Sidelobe reduction of circular arrays with a constant excitation amplitude," *IEEE Trans. Antennas Propag.*, vol. 25, no. 6, pp. 896–898, Nov. 1977.

[36] T. B. Vu, "Side-lobe control in circular ring array," *IEEE Trans. Antennas Propag.*, vol. 41, no. 8, pp. 1143–1145, Aug. 1993.

[37] A. Ip, D. R. Jackson, and A. A. Oliner, "An improved calculation procedure for the radiation pattern of a cylindrical leaky-wave antenna of finite size," *IEEE Trans. Antennas Propag.*, vol. 40, no. 1, pp. 19–24, Jan. 1992.

[38] H. Ostner, E. Schmidhammer, J. Detlefsen, and D. R. Jackson, "Radiation from dielectric leaky-wave antennas with circular and rectangular apertures," *Electromagn.*, vol. 17, no. 5, pp. 505–535, 1997.

[39] O. Luukkonen, C. Simovski, G. Granet, G. Goussetis, D. Lioubtchenko, A. V. Raisanen, and S. A. Tretyakov, "Simple and accurate analytical model of planar grids and high–impedance surfaces comprising metal strips or patches," *IEEE Trans. Antennas Propag.*, vol. 56, no. 6, pp. 1624–1632, Jun. 2008.

[40] D. Comite, P. Baccarelli, P. Burghignoli, and A. Galli, "Omnidirectional 2-D leaky–wave antennas with reconfigurable polarization," *IEEE Antennas Wireless Propag. Lett.*, vol. 16, pp. 2354–2357, 2017.

[41] D. Comite, P. Burghignoli, P. Baccarelli, D. Di Ruscio, and A. Galli, "Equivalent-network analysis of propagation and radiation features in wire-medium loaded planar structures," *IEEE Trans. Antennas Propag.*, vol. 63, no. 12, pp. 5573–5585, Dec. 2015.

[42] David E. Muller, "A method for solving algebraic equations using an automatic computer," *Math. Tables Aid. Comput.*, vol. 10, no. 56, pp. 208–215, 1956.